Investigation of land ice-ocean interaction with a fully coupled ice-ocean model: Part 2. Sensitivity to external forcings

Investigation of land ice-ocean interaction with a fully coupled ice-ocean model: 2. Sensitivity to external forcings

D. N. Goldberg,[1] C. M. Little,[2] O. V. Sergienko,[3] A. Gnanadesikan,[4] R. Hallberg,[5] and M. Oppenheimer[2]

Received 11 October 2011; revised 11 May 2012; accepted 18 May 2012; published 29 June 2012.

[1] A coupled ice stream-ice shelf-ocean cavity model is used to assess the sensitivity of the coupled system to far-field ocean temperatures, varying from 0.0 to 1.8°C, as well as sensitivity to the parameters controlling grounded ice flow. A response to warming is seen in grounding line retreat and grounded ice loss that cannot be inferred from the response of integrated melt rates alone. This is due to concentrated thinning at the ice shelf lateral margin, and to processes that contribute to this thinning. Parameters controlling the flow of grounded ice have a strong influence on the response to sub-ice shelf melting, but this influence is not seen until several years after an initial perturbation in temperatures. The simulated melt rates are on the order of that observed for Pine Island Glacier in the 1990s. However, retreat rates are much slower, possibly due to unrepresented bedrock features.

Citation: Goldberg, D. N., C. M. Little, O. V. Sergienko, A. Gnanadesikan, R. Hallberg, and M. Oppenheimer (2012), Investigation of land ice-ocean interaction with a fully coupled ice-ocean model: 2. Sensitivity to external forcings, *J. Geophys. Res.*, *117*, F02038, doi:10.1029/2011JF002247.

1. Introduction

[2] Heat contained in the Southern Ocean has the potential to influence the evolution of the grounded portion of the Antarctic Ice Sheet. The pattern of ice shelf thinning in the Amundsen Sea embayment in recent decades [*Rignot*, 1998; *Rignot et al.*, 2002; *Shepherd et al.*, 2002, 2004], as well as the observed speedup and thinning of the ice streams feeding those shelves, has been largely attributed to ocean-induced melting at the base of the ice shelves. The water at depth on the continental shelf, which derives from Circumpolar Deep Water (CDW) with temperatures greater than 3.5°C above the in-situ freezing point [*Jacobs et al.*, 2011], can generate area-averaged melt rates up to two orders of magnitude greater than those observed under larger Antarctic ice shelves [*Jacobs et al.*, 1996, 2011].

[3] Ocean conditions in and near ice shelf cavities are known to exhibit variability. Various bathymetric features enable the transport of warm water from the continental slope onto the continental shelf, and it is suggested that this transport is modulated by large-scale atmospheric variability on the annual and decadal timescale [*Thoma et al.*, 2008]. Large-scale trends in the heat content and/or thermocline depth of the Southern Ocean [*Jacobs*, 2006] may also have affected the properties of water on the continental shelf, or may do so in the future.

[4] One of the fastest-accelerating ice streams, Pine Island Glacier (PIG), Antarctica, has exhibited temporal variability on the decadal scale as well [*Joughin et al.*, 2003], but this may have been for reasons other than forcing from continental shelf temperatures. Establishing a direct connection between historical trends in ocean temperature and glaciological behavior requires an understanding of the response of the coupled system.

[5] We briefly mention some notable modeling investigations of the relationship between ocean conditions and sub-ice shelf basal melting (for a more detailed account, see *Holland et al.* [2008]). Many previous modeling studies considered ocean circulation under static ice shelves, and of those, many found a power law relationship between temperature and melt rates [*MacAyeal*, 1984; *Jenkins*, 1991; *Hellmer et al.*, 1998; *Holland et al.*, 2008; *Little et al.*, 2009]. In studies that included a dynamic ice shelf, a linear relationship between melt rates and ocean temperature was observed [e.g., *Grosfeld and Sandhager*, 2004; *Walker and Holland*, 2007] (but this may have been due to the narrow

[1]Department of Earth, Atmospheric and Planetary Sciences, MIT, Cambridge, Massachusetts, USA.
[2]Woodrow Wilson School of Public and International Affairs, Princeton University, Princeton, New Jersey, USA.
[3]Department of Atmospheric and Oceanic Sciences, Princeton University, Princeton, New Jersey, USA.
[4]Department of Earth and Planetary Sciences, Johns Hopkins University, Baltimore, Maryland, USA.
[5]Geophysical Fluid Dynamics Laboratory, NOAA, Princeton, New Jersey, USA.

Corresponding author: D. N. Goldberg, Department of Earth, Atmospheric and Planetary Sciences, MIT, 77 Massachusetts Ave., Cambridge, MA 02139, USA. (dgoldber@mit.edu)

0148-0227/12/2011JF002247

Table 1. Far-Field (and Initial) Ocean Layer Temperatures (in Degrees C) in the Various Coupled Experiments

Layer	Upper Interface Elevation	0°C Experiment	0.6°C Experiment	1.2°C Experiment	1.8°C Experiment
1	0 m below surface	−1.9	−1.9	−1.9	−1.9
2	5 m below surface	−1.9	−1.9	−1.9	−1.9
3	10 m below surface	−1.8	−1.8	−1.8	−1.8
4	−300 m	−0.9	−0.6	−0.3	0.0
5	−700 m	0.0	0.6	1.2	1.8

range of temperatures considered). It should be pointed out, however, that neither of these studies allowed for grounding line migration or evolution of the flow of grounded ice inland of the ice shelves, thereby preventing the assessment of overall ice sheet response. *Walker and Holland* [2007] noted that adjustment of grounded thickness might have further modified ice geometry and changed their model results.

[6] Taking the view that propagation of thickness change into the ice sheet interior is the glaciologically important result of ocean temperature forcing, we extend the question of the relationship between ocean temperature and melt rates, and ask whether grounding line retreat or loss of grounded ice volume responds to ocean temperature forcing in a direct way. Specifically, we aim to address the following questions: can grounded ice response to ocean temperatures be fit to a power law relation similar to that found for melting under a static shelf? Can small changes in deep ocean temperatures lead to large changes in grounded ice response? Does grounded ice response depend primarily on large-scale patterns of the sub-ice shelf melt rate field, or is it sensitive to spatial variability of melt rates?

[7] In this study, an ice shelf-ice stream system is exposed to basal melting calculated from a three-dimensional ocean model. We use a new ice stream-ice shelf-ocean coupled model, which is introduced in *Goldberg et al.* [2012]. The model is capable of capturing the long-term adjustment of the coupled system, including movement of the grounding line, changes in ice shelf cavity geometry, and changes in the volume of grounded ice. In this study, we focus on the sensitivity of the long-term ice sheet response to oceanic forcing, and leave the temporal aspect of ocean variability for future investigations. Multiple experiments are carried out with different far-field ocean conditions, and different choices of the parameters controlling grounded ice flow.

[8] The results presented here are intuitive in the sense that stronger thermal forcing leads to more sub-ice shelf melting and more grounding line retreat. However, a strongly nonlinear response is seen in grounded ice evolution, which is not observed in melt rates. Examination of the coupled response reveals a complicated, nonlocal interaction between melting and ice flow within the ice shelf. Furthermore, while the parameters controlling grounded ice flow exhibit a strong influence on the long-term grounded response to melting, the short-term response of grounded ice volume is found to be somewhat insensitive to grounded ice flow parameters.

2. Far-Field Temperature Sensitivity

2.1. Experimental Setup

[9] A detailed description of the coupled model is presented in *Goldberg et al.* [2012]. The experiments discussed in this section all use the same domain, bathymetry, boundary and initial conditions, and grounded and material parameters of ice (e.g., input flux q_0, basal traction β^2, and Glen's law parameter A).

[10] Four different experiments are run, each corresponding to a different far-field temperature/salinity profiles. The profiles at depth were generated by considering two end-members: the cold fresh water generated by wintertime convection ("Winter Water"),and the warmest water observed on the Amundsen Shelf in a recent oceanographic study [*Jacobs et al.*, 2011], relatively unmodified CDW. The temperature and salinity are −1.8°C and 34 psu for the former, and 1.3°C and 34.73 psu for the latter. Three different ratios of the two water masses were considered, contributing to different properties for the bottom layer (this is similar to *Determann et al.* [2012], in which different bottom temperatures were considered). The different temperature and salinity profiles are given in Tables 1 and 2. The experiments are named according to the temperatures of the bottom ocean layers, i.e., 0.0, 0.6, and 1.2°C. Additionally, an extreme case was considered in which the bottom is much warmer than observed on the continental shelf; this is the 1.8°C experiment. The first three experiments are meant to represent differing amounts of CDW being transported on to the shelf; the last represents an increase in temperature of the water being transported. The 0.6°C experiment is that discussed in *Goldberg et al.* [2012].

[11] We justify the 1.8°C experiment based on warming trends have been reported in the Southern Ocean over the second half of the twentieth century (though their origin is debatable [*Jacobs*, 2006]). Additionally, modeling studies that show century-scale warming at depth in the Southern Ocean under climate warming scenarios [*Schewe et al.*, 2011; *Yin et al.*, 2011]. While we make no claim as to conditions on the Amundsen shelf in the coming centuries, we are nonetheless interested in assessing the potential impact of warming on our coupled system.

[12] The initial state is that of an ice stream-ice shelf system run to equilibrium in the absence of the ocean model. The experiment then begins by initiating model coupling, and the ice shelf is exposed to submarine melting. Ocean temperature forcing is kept constant (for a given experiment), and the model is run until a new approximate steady state is reached, which occurs on the timescale of centuries.

Table 2. Far-Field (and Initial) Ocean Layer Salinities (in psu) in the Various Coupled Experiments

Layer	0°C Experiment	0.6°C Experiment	1.2°C Experiment	1.8°C Experiment
1	33.0	33.0	33.0	33.0
2	33.1	33.1	33.1	33.1
3	34.0	34.0	34.0	34.0
4	34.21	34.28	34.35	34.37
5	34.42	34.57	34.71	34.74

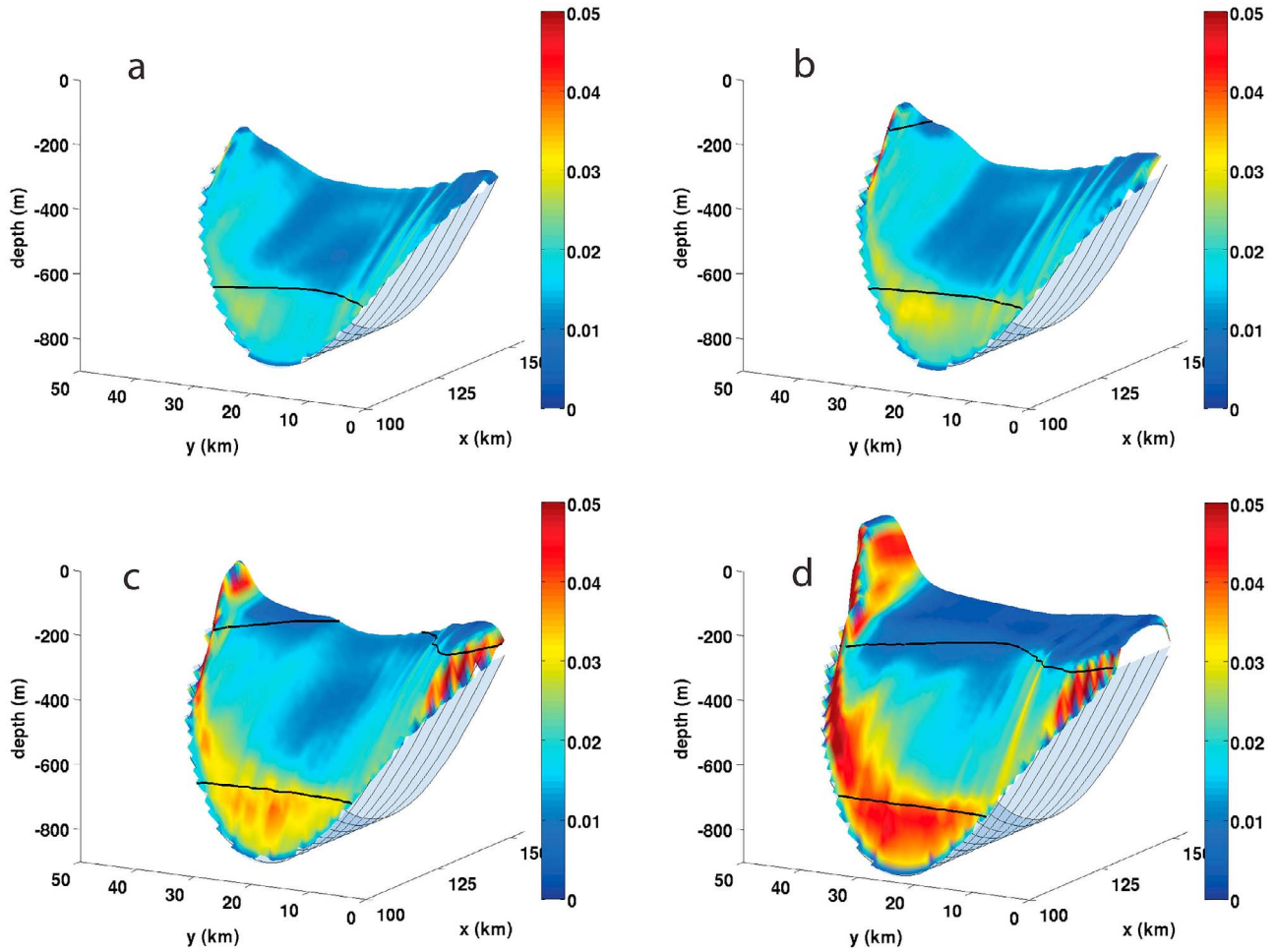

Figure 1. Final steady state ice shelf cavity geometries in temperature sensitivity study. (a) 0.0°C, (b) 0.6°C, (c) 1.2°C, and (d) 1.8°C experiments. The upper surface is ice shelf basal elevation, and lower surface is bedrock elevation. Coloring is the magnitude of basal slope. The perspective is from the grounded ice domain, looking seaward. Thick contours denote the 700 m and 300 m depth contours.

2.2. Results

[13] The ice shelf cavity geometries of the coupled steady states are shown in Figure 1. Higher slopes and higher basal elevations (corresponding to thinner shelves) are seen with higher ocean temperatures. Toward the ice shelf front there is an asymmetry between lateral margins, with the Coriolis-favored margin (in the Southern Hemisphere) being thinned to form a channel. The channel is more pronounced at higher ocean temperatures (Figure 3b), and at the highest ocean temperature forcing (1.8°C), the channel cuts almost through the shelf.

[14] In terms of sub-ice shelf melt rate patterns, certain qualities are common to all of the experiments (Figure 2). As discussed in *Goldberg et al.* [2012], ice shelf basal slope exerts a strong control on melt rates where the mixed layer is thin, which is most of the area of the ice shelf outside of the boundary current on the Coriolis-favored side. Background stratification is equally important. In Figures 1 and 2 thick contours denote the 700 m and (if present) the 300 m depth contours, which are, respectively, the upper surfaces of the warmest and second-warmest layers in the far-field temperature profile. High-slope regions form over the depth interval where warm water is available for entrainment. But within the high-slope regions there is spatial variability in melt rate that is determined strongly by slope magnitude. The maximum melt rate does not occur at the grounding line (at least not at the deepest part), but a few kilometers downstream. Higher ocean temperature moves this maximum closer to the grounding line. However, the exact position of the melt-rate maximum is controlled by a number of factors, including the local slope (which changes as a function of distance from the grounding line between simulations) and the path taken by the mixed layer from the grounding line. Thus it is difficult to attribute the position or magnitude of the melt-rate maximum to any single factor. In the boundary currents, where advective heat transport is important and a convergence-thickened mixed layer shields temperatures from cooler interior water, melt rates are higher than outside the currents.

[15] It can also be seen from Figure 2 that the experiments involve different levels of grounding line retreat; this is explored below, but first we discuss aspects of ice shelf geometry in the sensitivity experiments. From centerline profiles (Figure 3a), aslope break can be seen clearly at

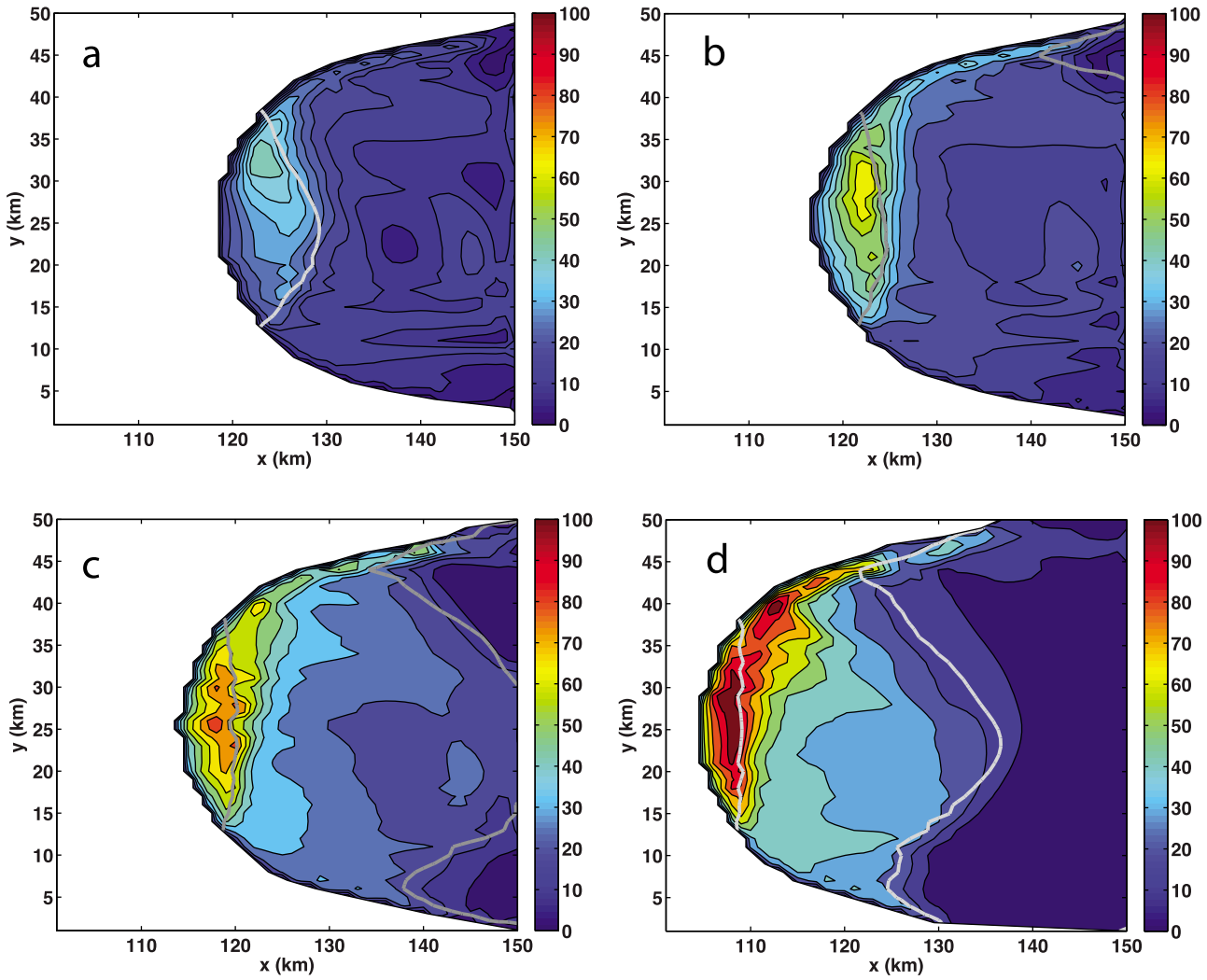

Figure 2. Final steady state melt rate fields in temperature sensitivity study (in meters per year). (a) 0.0°C, (b) 0.6°C, (c) 1.2°C, and (d) 1.8°C experiments. Thick gray contours are the 700 m and 300 m depth contours.

~700 m depth, corresponding to warmer interior ocean layers at depth. Slopes below 700 m increase from 0°C to 1.2°C forcing, but less so for the increase to 1.8°C. Transverse basal profiles (Figure 3) highlight the longitudinal channel referred to above, which increases in amplitude with far-field ocean temperature.

[16] In the 1.8°C experiment the margin has ungrounded and thinned almost completely. It appears that the shelf thins almost to zero in the 1.8°C case. In fact, the model was modified to disallow melting where the shelf thinned below 10 m, because the ice shelf velocity solver as written requires nonzero thickness everywhere. However, ice this thin carries very little stress and we consider it to be thinned to zero for the purposes of the experiments reported here.

[17] Transient evolution of the sensitivity study is shown in Figure 4. In each run, there is an initial dropoff in total (areally integrated) melt rate (Figure 4c) over the initial 2–3 years of integration. *Goldberg et al.* [2012] attributes this to a shrinking of the area exposed to warm water due to the development of the region of high slope, despite the fact that melt rates in the high-slope region increase. There then follows a period of increasing melt rates when features develop downstream of the high-slope region due, in part, to the interaction between ice shelf advection and basal slope-driven melting (for more details see *Goldberg et al.* [2012]). This transient increase becomes stronger as ocean temperature increases. However, at long times, the incremental increase in total melt rate (that is, the difference in melt rate per increment in ocean temperature forcing) decreases with forcing. The transient increase in total melt rate is not due to change in ice shelf area, as average melt rates follow similar trajectories.

[18] Figure 4a shows $x_{g,\min}$, the most upstream extent of the grounding line, and Figure 4b plots trajectories of Volume Above Floatation, or *VAF*, defined by

$$VAF = \int_G \left[h - \left(-\frac{\rho_w}{\rho_i} R(x,y) \right)_+ \right] dA \qquad (1)$$

(integration is over the grounded portion of the domain (G), and the "+" subscript indicates the positive part). The rate of change of *VAF* (Figure 4d) is ideal for assessing grounded

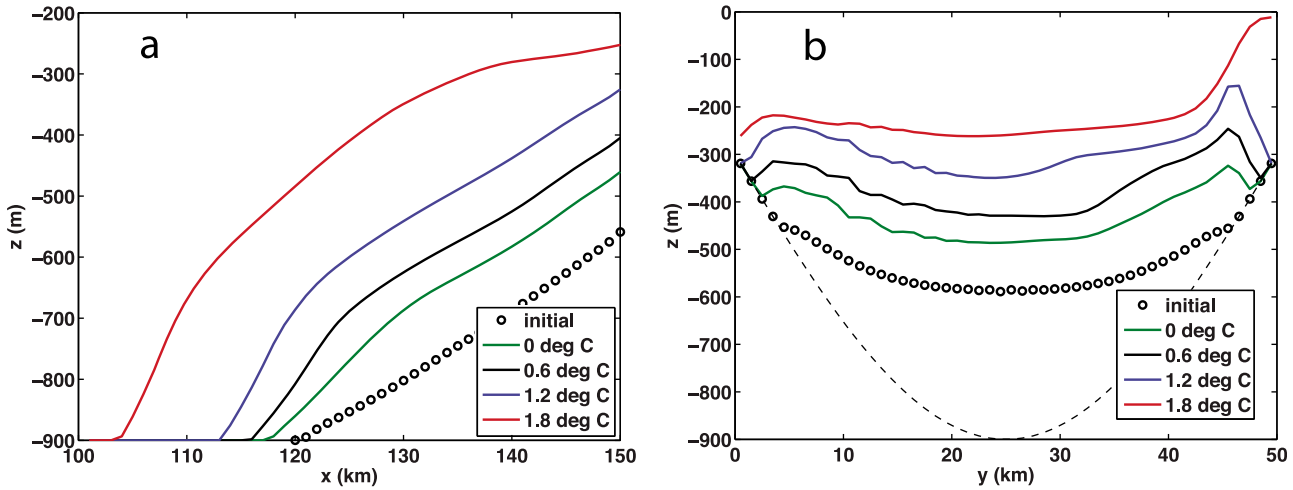

Figure 3. Profiles of steady state ice shelves in the sensitivity experiment. (a) Ice shelf draft (basal elevation) on a longitudinal profile along the center line (y = 25 km). (b) Ice shelf draft along a transverse profile at the ice shelf front. Dashed line in Figure 3b is bed elevation.

ice response. Its characteristic trajectory seen in the experiments, a quick increase followed by a gradual decrease in loss rate, is due to a relatively quick coupled adjustment of ice shelf thickness, followed by a long period of shelf lengthening. These shelf geometrical changes lead to shifts in the stress balance, affecting mass flux at the grounding line. The incremental response in maximum loss rate (the difference in maximum loss rate per increment in ocean temperature forcing) increases as ocean temperatures increase, with the 1.2°C→1.8°C incremental response being almost twice as large as the 0.6°C→1.2°C incremental response. The same behavior is not observed in spatially integrated melt rate, although the response in maximum *VAF* loss rate can be somewhat explained by melt rate history, which we examine more closely in section 3.2.

[19] The long-term grounding line position and *VAF* response show a behavior that is not commensurate with that of integrated melt rates. With an increase in temperature from 1.2 to 1.8°C, the incremental long-term integrated melt rate response is diminishing. However, while all other runs have dramatically slowed their retreat after 100 years, the 1.8°C run has a 2 century-long tail during which *VAF* loss rates remain substantial (∼1 km^3/a). This long tail in the recovery is a qualitatively different response than seen in the other runs. Additionally, grounding line retreat is nearly twice that of the 1.2°C run. Whether or not the 1.8°C run actually finds a steady state (i.e., whether the system is stable with the given forcing) was not verified since computational considerations prevented the simulation from being run for longer than 400 years.

[20] Another difference between the 1.8°C experiment and the other experiments is the apparent noisiness of the melt rate trajectory. This may be due to rapid adjustment of the shelf and grounding line driving small differences in the melt rate. However, it could also reflect an issue with the setup of the coupled model. The underlying assumption of the coupled model is that the melt rate field reaches a unique steady state (for a given shelf geometry and far-field profile) after a 10–15 day spin up of the ocean model. It may be the case that, with such strong far-field ocean forcing and associated vigorous circulation, the ocean needs more time to reach such a state. However, the fact that the "noise" diminishes when the *VAF* loss rate becomes small, suggests that it is in part due to modification of the ice shelf cavity. We emphasize, however, that our intention with this study was to explore the bounds of the parameter space involved. Additionally, we are confident that much of the noise seen in the melt rate is smoothed out by the ice model, and that any possible truncated ocean adjustment is not responsible for the nonlinear response described above.

[21] A characteristic common to all the simulations, including the 1.8°C experiment, is the fact that they all reach their maximum rate of *VAF* loss after about a decade. This is curious since the pattern and magnitude of melting, as well as the thinning of the shelf, are very different across the experiments. It suggests a factor common to all experiments that is influencing this turning point. In section 4 we explore this dependence on grounded ice parameters further.

[22] It should be emphasized that the bedrock topography chosen influences the grounded ice response we observe. With a bed that deepens inland, the backstress required to slow retreat would increase as the grounding line moved inland, and there would be potential for unstable retreat with a sufficiently steep slope [e.g., *Weertman*, 1974; *Thomas*, 1979; *Schoof*, 2007; *Goldberg et al.*, 2009]. The deepening of the cavity, exposing more of the shelf to warm water, would be an additional positive feedback. The purpose of our study was not to investigate the marine ice instability, and so we did not choose a fore deepened bed. But it should be noted that with different bed configurations steady states would not necessarily be realized, particular for warmer ocean temperatures.

3. Discussion of Sensitivity to Ocean Temperature

3.1. Melt Rate Response

[23] Various studies examine the response of ice shelf basal melt rate to changes in far-field or interior ocean temperatures. Studies that involve a static shelf have suggested a power law response with exponent greater than

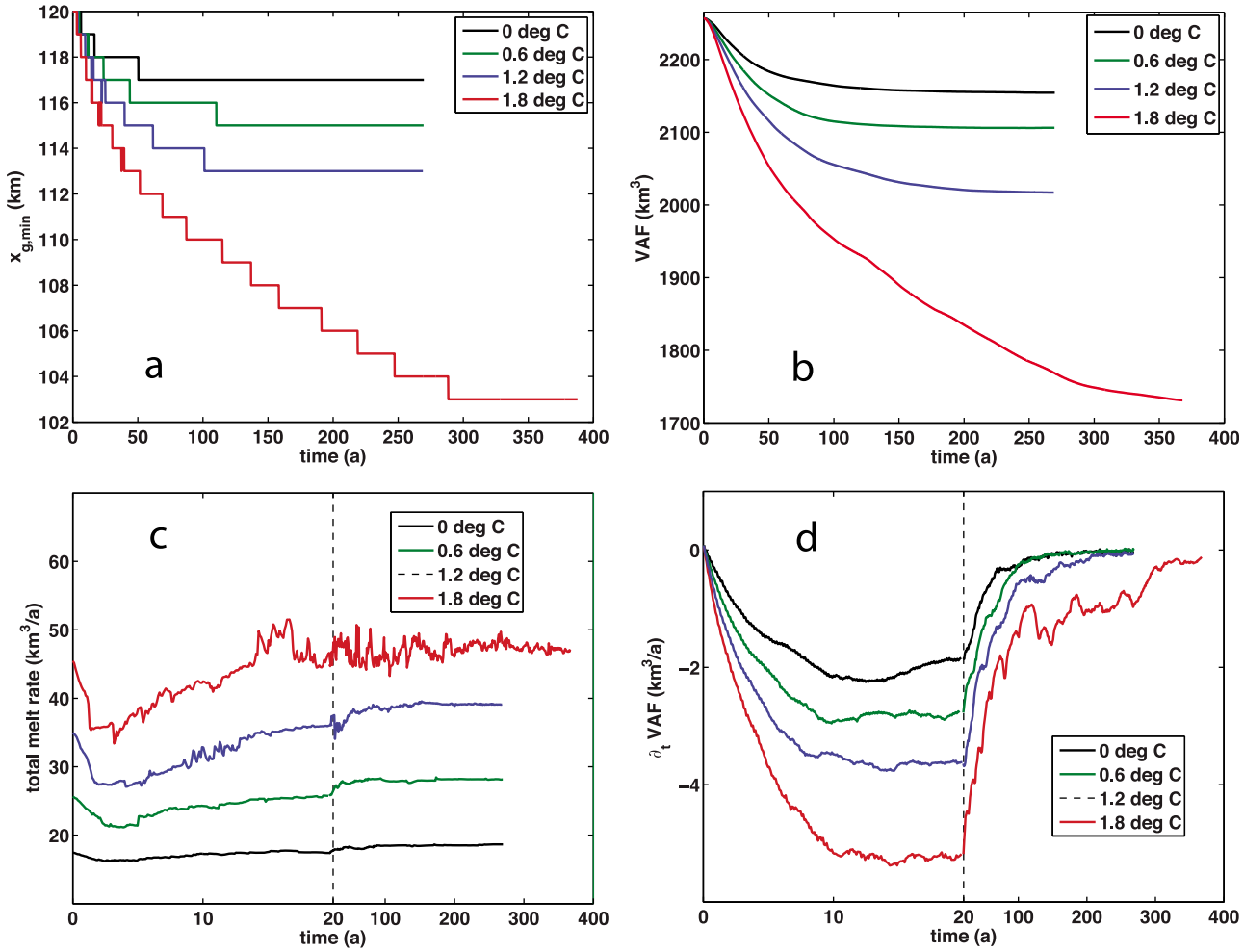

Figure 4. Transient evolution for the simulations in the far-field temperature sensitivity experiment. (a) Minimum grounding line position (x_g). (b) Volume above floatation (*VAF*). (c) Spatially integrated melt rate. (d) *VAF* loss rate. For melt rates and *VAF* loss rates, the time axis is distorted so the adjustment over the first 20 years can be seen more clearly. Note the difference in response between the 1.8°C experiment and the others with respect to x_g and *VAF*, in contrast to total melt rate.

unity. For example, *MacAyeal* [1984] and *Holland et al.* [2008] argue for a quadratic response on a theoretical basis (*Holland et al.* [2008] also provide corroborating numerical evidence).

3.1.1. Static Shelf Response

[24] We first examine the response of melt rates to ocean temperature forcing with a static ice shelf geometry, by comparing maximum and average melt rates with thermal forcing in the first coupled timestep of the sensitivity study (since all runs begin with the same ice shelf geometry). It is not straightforward which value to use for thermal forcing, since the melting point depends on pressure and salinity. Also, the imposed temperature profile varies with depth, with the warmest water being below 700 m (in contrast, the temperature in the imposed profiles of *Holland et al.* [2008] was uniform below 200 m). We expect the highest melt rates to be below this depth, where pressure is high enough to depress the melting point nearly a degree relative to the surface. Thus we consider a surface melting point of −1.8°C, a pressure-depth slope of 10^{-3} °C/m, and a representative depth of 800 m, and subtract the resulting characteristic melting point $T_{m,800}$ from the lowest-layer temperature T_D. Maximum and area-averaged melt rate are shown with data points in Figure 5a (results from our coupled experiments are supplemented with static-shelf runs at lower temperatures in order to test for a quadratic fit over a wide temperature range).

[25] The relationship between thermal forcing and melt rates (both average and maximum) is fit well by a parabola. This is visually apparent from the data, but we quantify this fit by calculating the adjusted R^2 coefficient for least squares fits to both linear and quadratic functions. The adjusted R^2 coefficient takes into account the additional degree of freedom in a quadratic fit [*Glantz and Slinker*, 2001]. For average melt rate, the coefficient is 0.964 for a linear fit, while it is 0.9998 for a quadratic fit. The linear and quadraric adjusted R^2 coefficients compared similarly for maximum melt rate. The quadratic best-fit curves pass close to the origin, which is reasonable, while the linear best-fit curves do not. However, this may be as a result of our choice for thermal forcing.

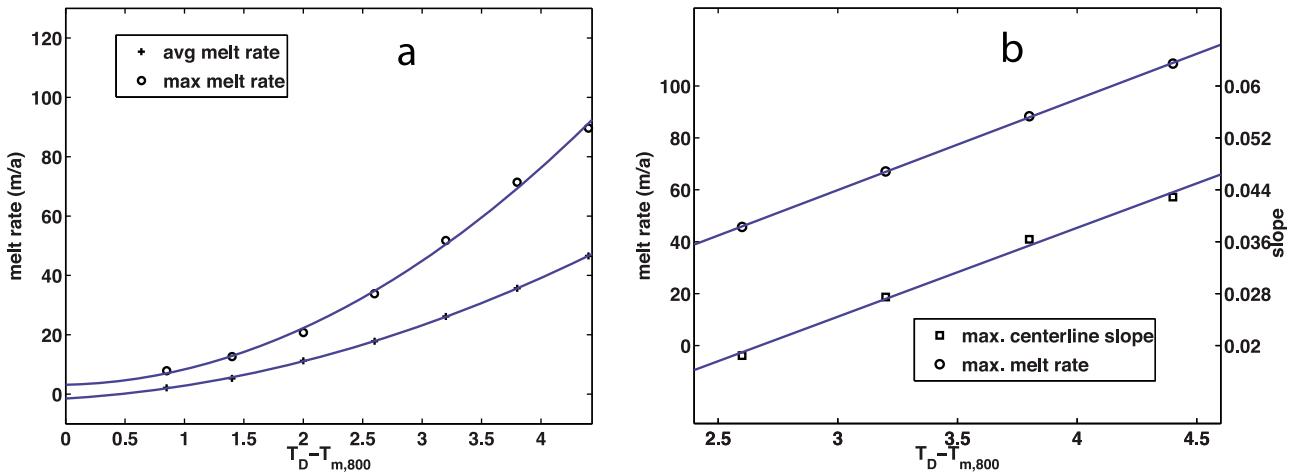

Figure 5. (a) Maximum and average melt rate against thermal forcing for a static shelf. Data points are shown with best-fit parabolas. (b) Maximum melt rates and slopes (longitudinal, along y = 25 km) for steady states of coupled simulations. Best-fit lines are shown; the range is too small to evaluate a quadratic fit.

3.1.2. Melt-Slope Dependency

[26] Implicit in the melt-temperature relation under an ice shelf is a dependence on the slope of the ice shelf base, such that higher basal slopes lead to faster mixed layer velocities and higher entrainments rates and thus higher melt rates [e.g., *Holland et al.*, 2008; *Little et al.*, 2009]. As basal slope changes over the course of the experiments (cf. Figure 3a), it is reasonable to assume this might lead to an even stronger melt rate response than that found under a static shelf. Figure 5b plots maximum steady state melt rate in the temperature sensitivity experiment, as well as maximum longitudinal slope along the center line y = 25 km, which is a close proxy for slopes below ~700 m depth (due to differing ice shelf extents, it is not reasonable to compare spatially averaged melt rates). For a given ocean temperature, maximum melt rate increases from its initial value (as does slope).

[27] Unfortunately, the range of ocean temperature forcing does not allow as complete a regression analysis as is done in section 3.1.1. In fact, one cannot distinguish between a quadratic and linear fit from only the four rightmost points in Figure 5a (those that correspond to the coupled experiments). Still, it is apparent that maximum melt rate does not exhibit a stronger response to temperature forcing than that seen for a static shelf, even though basal slope increases (at least) linearly. However, this does not contradict the idea that basal slope controls melt rates, as the dependency on slope is complex and nonlocal. For example, the basal area exposed to the warmest water decreases with slope, possibly decreasing the length of the path a plume takes while directly exposed to the bottom ocean layer. This may limit the heat available for entrainment (and thus for melting) downstream, where mixed layer velocities are highest, thus shifting the melt rate maximum upstream and weakening its magnitude. We also note that, in our experiments, an increase in bottom-layer temperature is accompanied by an increase in salinity, making interior layers denser and possibly inhibiting entrainment (however, the salinity increase corresponding to the 1.2→1.8°C temperature increase is small).

3.2. Grounded Ice Response

3.2.1. Short Term Grounded Response

[28] In section 2.2 some peculiarities of the incremental response of grounded ice when the forcing (T_{bot}) is increased from 1.2 to 1.8°C were noted. For instance, the increase in maximum *VAF* loss rate (achieved after ~10 years)is disproportionate to the increase in maximum melt rate. This feature, however, is consistent with the total loss of ice shelf volume and the melt rate history. As noted in section 2.2, melt rates increase over the first decade in the 1.8°C run more quickly than in the others. Ice volume change over a given time period is a function of total volume input (which is constant here) minus total volume removed by melting and calving. Specifically,

$$\Delta V_{10} = I_{10} - M_{10} - C_{10} \tag{2}$$

where ΔV_{10} is total volume change of ice in the domain over the first 10 years of simulation; I_{10} is the total volume input at the upstream boundary; M_{10} is total melt (in volumetric terms); and C_{10} is total calved volume. As grounded ice volume change is negligible for the first decade, ΔV_{10} is a good measure of ice shelf volume change. Column 7 of Table 3 shows that the increase in shelf volume change over the initial decade is twice as large when temperature is increased from 1.2 to 1.8°C as for increases at lower temperatures. The *VAF* loss rate at t = 10 years (column 9) has a comparable pattern.

[29] The increase in shelf volume loss can be largely attributed to the increase in total (spatially and temporally integrated) melting. It is tenuous to assume that loss of buttressing and increased grounded flux can be explained solely by ice shelf volume change, as the relationship between ice shelf geometry and grounding line velocities is very complicated and nonlinear. Still, we note that a recent study using a flowline model, *Little et al.* [2012] suggests that integrated ice shelf volume changes describe changes in buttressing fairly well. Thus we suggest that the strong response in grounded mass loss in the early decades of

Table 3. Ice Shelf Volume Change and Its Components (See Equation (2)) Over the First 10 Years of Simulation, and *VAF* Loss Rate After 10 Years[a]

Experiment	M_{10} (km^3)	Increase	C_{10} (km^3)	Decrease	$-\Delta V_{10}$ (km^3)	Increase	$-\partial_t VAF\|_{t=10}$ (km^3/a)	Increase
0.0°C	166	-	698	-	91.5	-	2.25	-
0.6°C	228	62	676	22	131	39.5	2.96	0.71
1.2°C	292	64	646	29	166	35	3.77	0.8
1.8°C	378	86	624	23	229	63	5.38	1.61

[a]Columns 3, 5, 7, and 9 state increase (or decrease) of value in preceding column per increase in ocean forcing temperature.

adjustment of the coupled system is due to the relatively fast increase of melt rates during that time.

3.2.2. Role of the Margin in Ice Shelf Buttressing

[30] While the strong grounded ice response of the 1.8°C run in the early decades of the simulation can be satisfactorily explained by examining melt rates and volume change in a spatially integrated sense, the same is not true of the long-term response. The incremental response (that is, the response to a 1.2°C→1.8°C increase in forcing) in both maximum and integrated melt rates is relatively small. Yet, while there is at most 5 km of grounding line retreat in the other simulations, the grounding line in the 1.8°C run retreats almost 20 km. Not unrelated is the fact that the *VAF* loss rate remains substantial for 2 centuries longer than in the other simulations.

[31] We offer a heuristic explanation: with no variability in parameters that control grounded ice flow, the response to increases in temperature forcing is entirely due to changes in ice shelf geometry. And the geometrical factor most likely responsible for the behavior described above is the deep channel at the Coriolis-favored margin, most evident in the steady state shelf geometry shown in Figure 1. Unlike the other runs, the melt channel cuts almost all the way through the ice column, ungrounding the ice shelf at that margin. A diagnostic experiment (i.e., one in which velocity is solved just once with a given ice thickness distribution) is carried out using this steady state ice geometry. Thickness is instantaneously (and artificially) increased to 200 m wherever thickness is below this threshold value. Since such thin ice is only found along the left-hand margin (Figures 1 and 3b), this adjustment only modifies ice thickness in the deep channel and does not greatly affect ice elsewhere. The result of this diagnostic experiment is that volume flux across the grounding line is decreased by almost 1 km^3/a, which is on the order of the *VAF* loss rate during the long "tai" of the simulation. By contrast, carving an (artificial) channel of similar dimensions and volume at the center of the ice shelf front has a negligible (+0.06 km^3/a) effect on grounded ice flux. These results suggest the effect of the channel at the ice shelf margin is not simply due to its effect on overall shelf volume or thickness, and that the effect of ice shelf thinning greatly depends on its location within the shelf.

[32] The extreme thinning at the Coriolis-favored margin in the 1.8°C simulation takes time to manifest: the first point at which the shelf is less than 100 m thick anywhere in the domain does not occur until ∼70 years into the run. Thus, it is plausible that the buttressing effectiveness along the Coriolis-favored margin is all but lost after about a century, and this is why the *VAF* loss rate in the 1.8°C experiment does not return to zero until long after the other simulations. *VAF* loss does not slow until sufficient grounding line retreat and shelf extension takes place such that sufficient shear stress (i.e., buttressing load) can be placed on the opposite ice shelf margin.

[33] Accepting that it is the ungrounding and deep thinning at the Coriolis-favored lateral margin that is responsible for the grounded response to the 1.8°C forcing, there is then a question of how this ungrounding and thinning arises. It is an ice-dynamical effect as there is no melting in grounded cells, but it must be related to transverse asymmetries in the melt rate, as there are no such asymmetries in bedrock or initial ice geometry. It could be due to a decrease of lateral transport of ice toward the margin as the shelf thins, the effect of which is amplified by thinning due to melting in the boundary current. But there is cancelation with decreasing along-flow divergence, so the reasons are difficult to assess. Ungrounding at the margin leads to increased shelf thinning: ice moves slowly near the margin due to the no-flow boundary condition imposed on ice velocities, and the shallow bedrock near the boundary ensures the shelf there is fed with relatively thin ice. Thus, although the melt rates acting on the ice shelf here are relatively small, they lead to large thinning over time. Thus, a trend that is continuous with respect to ocean forcing (thinning tendency in the grounded cells at the ice domain margin) may lead to a nearly discontinuous response.

[34] Note that our explanation for thinning at the margin, and its role in the grounded response of the 1.8°C run in comparison to the other simulations, may be specific to bed geometry, as well as our choice of a no-slip condition at the lateral boundaries. The no-slip boundaries are supposed to represent a region of slow-moving ice outside of the ice stream that is capable of supporting high levels of lateral shear stress. Additionally, weakening of shear margins due to crevassing could amplify the effect of lateral margin thinning. In future investigations we propose to extend our model domain in order to resolve this slow-moving ice, and to account for margin weakening, as such treatment may give different behavior.

[35] Several ice-only studies have parameterized ocean melt rates in order to assess the effects of strong submarine ice shelf melting on grounded ice [e.g., *Walker et al.*, 2008; *Gagliardini et al.*, 2010; *Joughin et al.*, 2010; *Little et al.*, 2012]. These parameterizations can capture strong melting toward the grounding line, which is clearly an important aspect of the melt rate field. However, the results here demonstrate that other features, i.e., high melt rates along lateral margins, can be important as well. Such features will need to be taken into account if melt paramaterizations are to be used to assess the response of ice streams to ice shelf basal melting.

3.2.3. Implications Regarding Temporal Ocean Variability

[36] The coupled ice-ocean response to a step change in ocean temperatures is expressed over a range of timescales.

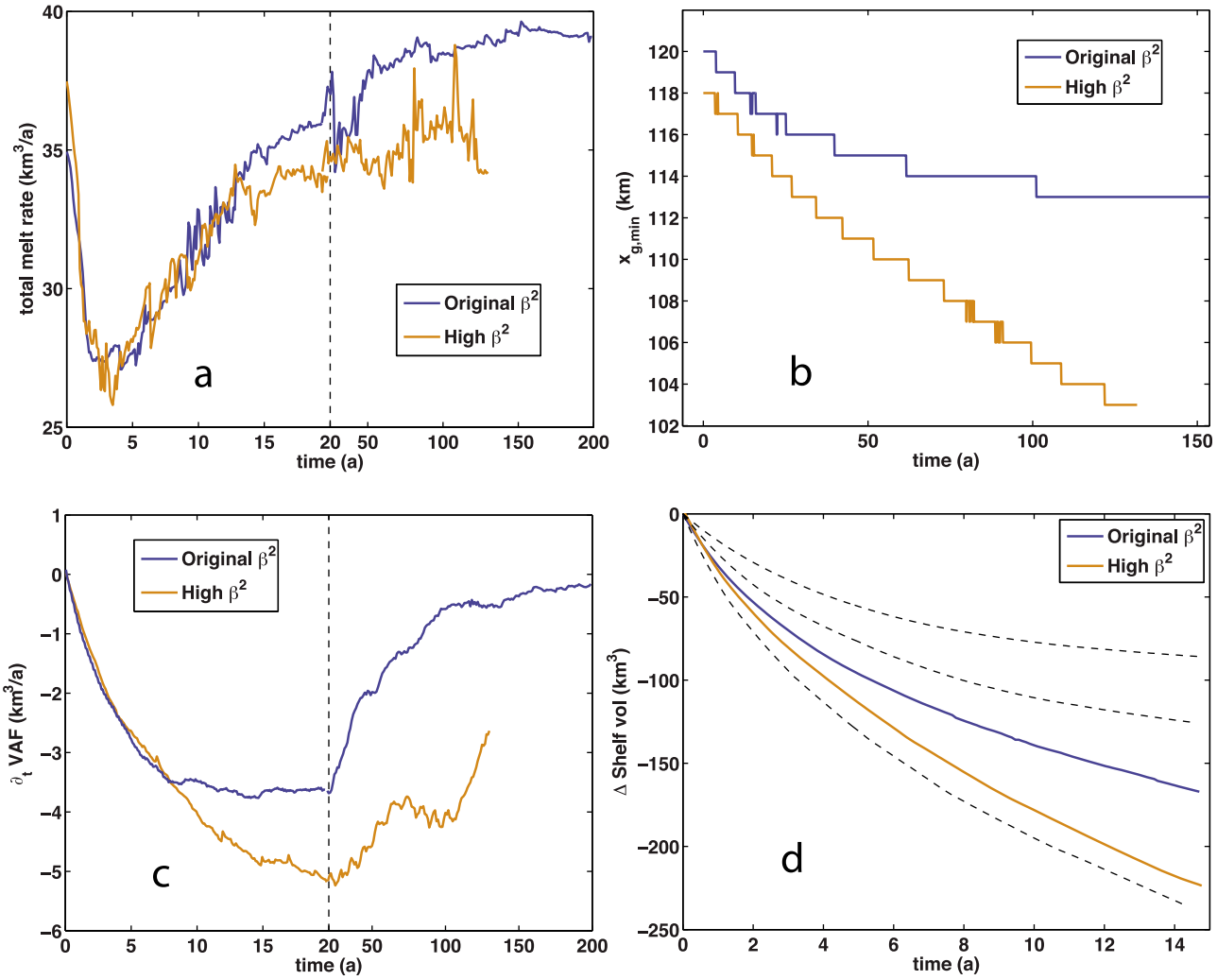

Figure 6. Transient evolution for the simulation in which basal traction (β^2) was varied. The corresponding simulation with the original β^2 is shown for comparison. (a) Integrated melt rate. (b) Minimum grounding line position (x_g). (c) *VAF* loss rate. (d) Shelf volume. Other experiments from the ocean temperature sensitivity study are shown in dashed lines for comparison (0.0°C, 0.6°C, and 1.8°C in descending order).

This means that the response of an ice shelf to realistic variability, which is likely to be expressed in terms of smoother changes, may occur at timescales different from those expressed by the ocean forcing. For instance, a fast (one- to several-year) oscillation in temperature might produce variability in basal slopes at the grounding line similar to that shown in Figure 3a. However, as the thinning is advected through the shelf the oscillation may be averaged out, so that it is unclear what the resulting grounded ice response would be. The response to temporal variations in ocean temperature forcing is a subject of future investigation.

4. Dependence on Grounded Ice Parameters

[37] In the temperature sensitivity experiment, parameters relating to the flow of grounded ice (input flux and β^2, or basal traction) were held constant, since our goal was to isolate the effects of changes in ocean properties. However, grounded parameters have also have a strong influence on the overall model response to submarine melting. To demonstrate this, an additional simulation was run, in which β^2 was increased from 9.6×10^8 to 20×10^8 Pa $(m/s)^{-1}$, making the bed more resistant to sliding (A, the Glen's law constant, was kept the same). This change necessitated a change in input volume flux of ice from the interior as well, in order to best make comparisons using a similar initial geometry, i.e., a similar initial shelf length. Considering that response to melting driven by under-shelf circulation was being studied, shelf length seemed the most appropriate metric for agreement of initial states. A 30% decrease in input flux yielded a balanced state of the uncoupled ice model with a grounding line position close to that of the other experiments. Aside from the change in grounded ice parameters, the experiment was conducted identically to the others. The far-field temperature and salinity of the 1.2°C experiment from the temperature sensitivity study were used to force the ocean model.

[38] This experiment was not run to steady state; rather, it was run only long enough to demonstrate the difference

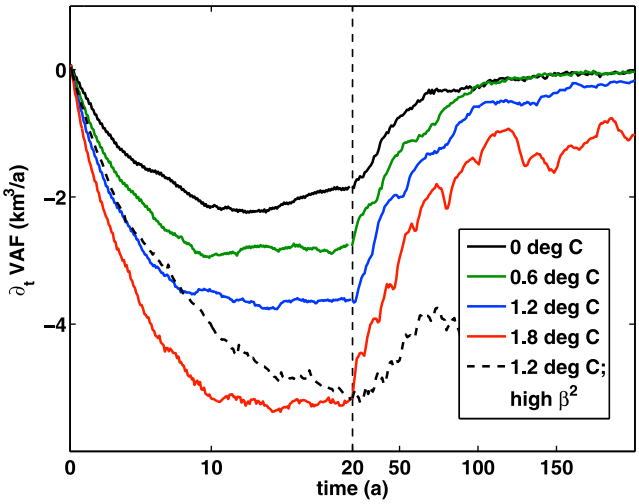

Figure 7. *VAF* loss rates for all experiments plotted on logarithmic timescale. For the experiments in the sensitivity study, there is a steady increase in loss rate until about 10 years, after which the loss rate decays. For the high basal traction experiment, which has the same ocean forcing as the 1.2°C experiment, the retreat continues for an additional ~6–8 years.

in grounded ice response. Transient results are compared against those from the 1.2°C experiment in Figure 6. It can be seen clearly that the high-β^2 (or, equivalently, low-sliding) experiment has a much higher retreat rate than the original experiment, despite the fact that integrated melt is slightly lower. The overall long-term results could have been anticipated from simple a priori considerations: in the low-sliding experiment there is less mass flux into the system at the upstream boundary, so comparable rates of mass loss (through melting) have a relatively larger effect. In other words, the slower the system throughput, the stronger the effect of a similar magnitude of melting.

[39] More intriguing, though, is the temporal expression of this difference in grounded response: the trajectories of x_g and *VAF* loss rate, as well as integrated melt rate, agree closely during the first decade before diverging. Correction for disagreement in x_g reveals that both runs have very similar ice shelf drafts in their initial states, with the largest differences close to the ice shelf front (not shown). This explains why integrated melt rates are initially comparable. However, it is curious that they remain so for over a decade: since the ice shelf in the low-sliding run is slower, similar melt rates lead to higher thinning rates, which can be seem from changes in ice shelf volume (Figure 6d), and one would expect melt rates to diverge.

[40] Changes in ice shelf volume are tied strongly to perturbations in grounded flux. However, the difference in shelf volume between the simulations does not manifest in *VAF* loss rates during the first decade. Indeed, the trajectory of ice shelf volume loss over the first decade is closer to that of the 1.8°C simulation, but *VAF* loss rates are closer to that of the 1.2°C simulation. There may be some compensation in terms of the stress balance. With a slower-moving shelf, tangential stress along its lateral margins is smaller, due to smaller lateral shearing rates. Buttressing therefore plays a smaller role in the stress balance, and so we expect that the grounded ice response to ice shelf thinning should not be as strong.

4.1. Timing of Retreat

[41] While all the experiments in the sensitivity study involved different rates of grounded mass loss, the rates reached their peaks, or came close to them, after about the same amount of time (a decade). This matches another timescale of the system: the residence time of an ice column within the ice shelf (as shown in *Goldberg et al.* [2012], ice shelf speeds do not change much in a relative sense during the initial decadal adjustment). On the other hand, in the slow-sliding experiment (with slower shelf velocities), it took about 20 years to reach this peak. While the residence time is only about 16 years, it can be seen that at this time the acceleration of *VAF* loss does slow (Figure 7).

[42] Both melting and advection of the resultant thinning contributes to the initial ice shelf adjustment following a perturbation, and shelf thinning leads to increased flux across the grounding line. Given the results of our coupled experiments, we speculate that grounded mass loss following a perturbation is rapid only for the length of time it takes the shelf to sweep out the new transients in ice shelf geometry, i.e., the residence time. After this point changes in ice shelf geometry occur on a slower timescale, set by changes in grounding line position and evolution of grounded ice (this is contingent on the grounding line retreat timescale being slow compared to the ice shelf residence time; see section 5 below). Note that in addition to its dependence on shelf velocities, residence time also depends on the size of the ice shelf, so the numbers here (10 years, 16 years) are specific to our setup.

5. Connection with Observed Behavior

[43] While our model neglects a number of processes (as detailed in *Goldberg et al.* [2012]), it is nonetheless informative to compare our results with recent observations of PIG. Average melt rates of 50 ± 10 m/a for the upstream 20 km of the PIG ice shelf (and 24 ± 4 m/a for the entire shelf) were inferred for the period from 1992–1996 [*Rignot et al.*, 2008], which is on the order of the melt rates seen in our experiments. However, grounding line retreat rates for the same period [*Rignot*, 1998] and (assuming mass input has not changed) grounded mass loss for the period from 1996–2007 [*Rignot*, 2008] were an order of magnitude larger than in our model. This suggests that something absent from our model was responsible for the high rates of grounding line retreat and grounded mass loss.

[44] Retreat over a bed that deepened inland would likely have led to greater grounded mass imbalances (since grounding line flux increases with bed depth) and faster grounding line retreat, and also higher melt rates due to more of the ice shelf being exposed to warm water [*Jacobs et al.*, 2011], but retreat rates an order of magnitude larger would likely require large bed slopes. *Jenkins et al.* [2010] suggests that the observed speedup and rapid retreat of PIG is due to retreat over a bathymetric ridge several decades ago. It is possible that localized bathymetric features of high basal slope could lead to short periods of rapid retreat in our model, but this needs investigation.

6. Conclusions

[45] Here, we have performed experiments with a coupled ice stream-ice shelf-ocean cavity model in which ocean temperature beyond the ice shelf front was varied between 0 and 1.8°C. Ocean temperature was seen to have a strong effect on sub-ice shelf melt rates, ice shelf geometry, and grounded ice response. Melt rates and ice shelf morphology differed in their response from that of grounded ice. As temperature was increased (by constant increments), the corresponding increase in terms of maximum melt rate and ice shelf basal slope was relatively constant (Figure 5b). On the other hand, loss of grounded ice showed a much stronger increase at the highest temperature forcing. In the long term (century scale), the strong response at high temperature forcing was likely due to concentrated melting and thinning in an area of the shelf that is important to the shelf's buttressing. Over the short term (decadal scale), it is not clear whether the spatial patterns of melting and thinning are more or less important than their spatial and temporal averages.

[46] For a single ocean temperature forcing, the basal stress coefficient of grounded ice was increased, which led to much larger rates of grounded ice loss than with the original basal stress coefficient. However, rates of grounded ice loss in the two simulations were very similar over the initial decade.

[47] Melt rates were on the order of those observed for PIG during the 1990s; however, mass loss and grounding line retreat rates were much slower. The reasons for this are unclear, but the fact that the bed in our model did not deepen inland or have any localized bumps or ridges may be a factor. However, we believe our findings are still useful, because they demonstrate the importance of ice shelf buttressing and spatial patterns of melting in the response of the coupled ice-ocean cavity system to warming.

[48] **Acknowledgments.** D.N.G. received funds from the Princeton AOS Postdoctoral and Visiting Scientist Program, and from NSF award ANT-1103375. C.M.L. received funds from the Princeton Carbon Mitigation Initiative. D.N.G. and C.M.L. received funds from the STEP program in the Woodrow Wilson School of Public and International Affairs, Princeton University. O.V.S. received funds from NSF awards ANT-0838811 and ARC-0934534. Stephen Price, Eric Larour, one anonymous reviewer, and editors Poul Christofferson and Bryn Hubbard contributed helpful comments to the manuscript. D. M. Holland and K. S. Smith kindly provided additional CPU time.

References

Determann, J., M. Thoma, K. Grosfeld, and S. Massmann (2012), Impact of ice-shelf basal melting on inland ice-sheet thickness: A model study, *Ann. Glaciol.*, *53*(60), 129–135, doi:10.3189/2012AoG60A170.

Gagliardini, O., G. Durand, T. Zwinger, R. C. A. Hindmarsh, and E. L. Meur (2010), Coupling of ice shelf melting and buttressing is a key process in ice sheet dynamics, *Geophys. Res. Lett.*, *37*, L14501, doi:10.1029/2010GL043334.

Glantz, S., and B. Slinker (2001), *Primer of Applied Regression and Analysis of Variance*, McGraw-Hill, New York.

Goldberg, D. N., D. M. Holland, and C. G. Schoof (2009), Grounding line movement and ice shelf buttressing in marine ice sheets, *J. Geophys. Res.*, *114*, F04026, doi:10.1029/2008JF001227.

Goldberg, D. N., C. M. Little, O. V. Sergienko, A. Gnanadesikan, R. Hallberg, and M. Oppenheimer (2012), Investigation of land ice-ocean interaction with a fully coupled ice-ocean model: 1. Model description and behavior, *J. Geophys. Res.*, *117*, F02037, doi:10.1029/2011JF002246.

Grosfeld, K., and H. Sandhager (2004), The evolution of a coupled ice shelf-ocean system under different climate states, *Global Planet. Change*, *42*, 107–132.

Hellmer, H., S. Jacobs, and A. Jenkins (1998), Oceanic erosion of a floating Antarctic glacier in the Amundsea Sea, in *Ocean, Ice, and Atmosphere: Interactions at the Antarctic Continental Margin*, *Antarct. Res. Ser.* vol. 75, edited by S. S. Jacobs and R. F. Weiss, pp. 83–99, AGU, Washington, D. C., doi:10.1029/AR075p0083.

Holland, P. R., A. Jenkins, and D. M. Holland (2008), The response of ice shelf basal melting to variations in ocean temperature, *J. Clim.*, *21*, 2558–2572.

Jacobs, S. S. (2006), Observations of change in the Southern Ocean, *Philos. Trans. R. Soc. A*, *364*, 1657–1681.

Jacobs, S. S., H. Hellmer, and A. Jenkins (1996), Antarctic ice sheet melting in the southeast pacific, *Geophys. Res. Lett.*, *23*, 957–960.

Jacobs, S. S., A. Jenkins, C. Giulivi, and P. Dutrieux (2011), Stronger ocean circulation and increased melting under Pine Island Glacier ice shelf, *Nat. Geosci.*, *4*, 519–523, doi:10.1038/NGEO1188.

Jenkins, A. (1991), A one-dimensional model of ice shelf-ocean interaction, *J. Geophys. Res.*, *96*, 20,671–20,677, doi:10.1029/91JC01842.

Jenkins, A., P. Dutrieux, S. S. Jacobs, S. D. McPhail, J. R. Perrett, A. T. Webb, and D. White (2010), Observations beneath Pine Island Glacier in West Antarctica and implications for its retreat, *Nat. Geosci.*, *3*, 468–472, doi:10.1038/ngeo890.

Joughin, I., E. Rignot, C. Rosanova, M. Lucchita, and J. Bohlander (2003), Timing of recent accelerations of Pine Island Glacier, Antarctica, *Geophys. Res. Lett.*, *30*(13), 1706, doi:10.1029/2003GL017609.

Joughin, I., B. Smith, and D. M. Holland (2010), Sensitivity of 21st century sea level to ocean-induced thinning of Pine Island Glacier, Antarctica, *Geophys. Res. Lett.*, *37*, L20502, doi:10.1029/2010GL044819.

Little, C. M., A. Gnanadesikan, and M. Oppenheimer (2009), How ice shelf morphology controls basal melting, *J. Geophys. Res.*, *114*, C12007, doi:10.1029/2008JC005197.

Little, C. M., D. N. Goldberg, A. Gnanadesikan, and M. Oppenheimer (2012), On the coupled response to ice-shelf basal melting, *J. Glaciol.*, *58*, 203–215.

MacAyeal, D. R. (1984), Thermohaline circulation below the ross ice shelf: A consequence of tidally induced vertical mixing and basal melting, *J. Geophys. Res.*, *89*, 597–606, doi:10.1029/JC089iC01p00597.

Rignot, E. (1998), Fast recession of a West Antarctic Glacier, *Science*, *281*, 549–551.

Rignot, E. (2008), Changes in West Antarctic ice stream dynamics observed with ALOS PALSAR data, *Geophys. Res. Lett.*, *35*, L12505, doi:10.1029/2008GL033365.

Rignot, E., D. G. Vaughan, M. Schmeltz, T. K. Dupont, and D. R. MacAyeal (2002), Acceleration of Pine Island and Thwaites Glaciers, West Antarctica, *Ann. Glaciol.*, *34*, 189–194.

Rignot, E., J. L. Bamber, M. R. van den Broeke, C. Davis, Y. Li, W. J. van de Berg, and E. van Meijgaard (2008), Recent Antarctic ice mass loss from radar interferometry and regional climate modelling, *Nat. Geosci.*, *1*, 106–110.

Schewe, J., A. Levermann, and M. Meinshausen (2011), Climate change under a scenario near 1.5°C of global warming: Monsoon intensification, ocean warming and steric sea level rise, *Earth Syst. Dyn.*, *2*, 25–35, doi:10.5194/esd-2-25-2011.

Schoof, C. (2007), Marine ice sheet dynamics. Part I. The case of rapid sliding, *J. Fluid Mech.*, *573*, 27–55.

Shepherd, A., D. J. Wingham, and J. Mansley (2002), Inland thinning of the Amundsen Sea sector, West Antarctica, *Geophys. Res. Lett.*, *29*(10), 1364, doi:10.1029/2001GL014183.

Shepherd, A., D. J. Wingham, and E. Rignot (2004), Warm ocean is eroding West Antarctic Ice Sheet, *Geophys. Res. Lett.*, *31*, L23402, doi:10.1029/2004GL021106.

Thoma, M., A. Jenkins, D. M. Holland, and S. S. Jacobs (2008), Modelling Circumpolar Deep Water intrusions on the Amundsen Sea continental shelf, Antarctica, *Geophys. Res. Lett.*, *35*, L18602, doi:10.1029/2008GL034939.

Thomas, R. H. (1979), The dynamics of marine ice sheets, *J. Glaciol.*, *31*, 347–356.

Walker, R. T., and D. M. Holland (2007), A two-dimensional coupled model for ice shelf-ocean interaction, *Ocean Modell.*, *17*, 123–139.

Walker, R. T., T. K. Dupont, B. R. Parizek, and R. B. Alley (2008), Effects of basal melting distribution on the retreat of ice-shelf grounding lines, *Geophys. Res. Lett.*, *35*, L17503, doi:10.1029/2008GL034947.

Weertman, J. (1974), Stability of the junction of an ice sheet and an ice shelf, *J. Glaciol.*, *13*, 3–11.

Yin, J., J. T. Overpeck, S. M. Griffies, A. Hu, J. L. Russell, and R. Stouffer (2011), Different magnitudes of projected subsurface ocean warming around Greenland and Antarctica, *Nat. Geosci.*, *4*, 524–528, doi:10.1038/ngeo1189.